Available online at www.sciencedirect.com
ScienceDirect
Journal of the European Ceramic Society 32 (2012) 1395–1403
www.elsevier.com/locate/jeurceramsoc

Oxidation behavior of electrically conductive α/β SiAlON composites with segregated network of TiCN

Ali Çelik, Erhan Ayas, Etem Halil, Alpagut Kara *

Department of Materials Science and Engineering, Anadolu University, Iki Eylul Campus, Eskişehir, Turkey

Available online 15 April 2011

Abstract

The oxidation behavior of novel electrically conductive α/β SiAlON composites with a continuous network of 2.5–10 vol% TiCN particulates was investigated. Composites, produced by coating spray dried granules with nano TiCN particles by a simple blending method, were gas pressure sintered at 1990 °C for 1 h under 10 MPa N_2 pressure. Oxidation tests were carried out between 800 °C and 1200 °C in air for 2 and 48 h in atmosphere of dry air. Below 1000 °C, the formation of TiO_2 crystals on the surfaces of TiCN particles was observed. Before the glass transition temperature of intergranular phase (T_g < 1000 °C), it was revealed that oxidation is controlled by the diffusion of oxygen into pre-formed TiO_2 particles. Above T_g, liquid glass dissolves the intergranular phase elements such as Ti, Y, and Si at the interface between TiCN and SiAlON particles. Migration of Ti towards the (opening point of the TiCN network) surface was found to be the main reason for the formation of subsurface porosity that slows down Ti diffusion through the surface. Moreover, it was detected that at high temperatures surface porosity filled by the intergranular glassy phase. Consequently, the oxidation rate was found to be decreased due to the slower oxygen diffusion.

Keywords: Composites; SiAlON; TiCN; Electrical conductivity; Oxidation

1. Introduction

Si_3N_4 and SiAlON ceramics are important structural materials due to their superior mechanical, thermal and chemical properties both at room and high temperatures. While wear resistance, hardness, toughness and creep resistance of Si_3N_4/SiAlON can be improved considerably by the dispersion of the secondary carbides, nitrides or borides,[1–7] electrical properties can also be improved by the addition of some functional phases.[8–13] Conductive Si_3N_4/SiAlON based composites are candidate materials for the applications such as heat exchangers, heaters, ignitiors that operates at high temperatures containing oxygen and/or oxidant substances (water vapor and carbon dioxide oxygen atmosphere). Therefore, the behavior of these composites against to oxygen at high temperatures is critical and has been subjected to a series of studies.[14–20]

TiN and TiCN particulates are the most preferred reinforcing phases to make Si_3N_4/SiAlON ceramics electrically conductive due to not only low electrical resistivity but also unique combination of mechanical properties. There are various approaches to produce such composites. The most common method is the direct dispersion of TiN/TiCN particles in Si_3N_4 matrix by conventional powder processing routes.[7–9] In these types of composites, homogeneous dispersion of minimum amount of secondary phase without degrading densification and mechanical features is very critical, since it affects the electrical conductivity. However, the dispersion of a secondary phase is a difficult task to achieve. Therefore, in situ formation of homogeneously distributed nano conductive particles is an alternative method to this approach.[21–23] Obtaining good electrical conduction by this method is also challenging, since process parameters must be controlled precisely to avoid the grain growth and accordingly separation of conductive particles from each other. A new method to obtain a continuous network in these types of composites has been developed by Ayas and Kara.[24] In this method, spray dried SiAlON granules with an average diameter of 100 μm were coated with nano-TiCN particles by dry mixing of these two components. Consequently, low resistivity values ($\approx 10^{-2}$ Ω m) were achieved with the incorporation of as low as 5 vol% of TiCN after gas pressure sintering.

For such ceramics, it is important to evaluate the thermal stability and degradation of mechanical and functional properties of such composites at high temperatures. In the present work, oxidation behavior of α/β SiAlON composites with different

* Corresponding author. Tel.: +90 222 3213550-6584; fax: +90 222 3222943.
E-mail address: akara@anadolu.edu.tr (A. Kara).

0955-2219/$ – see front matter © 2011 Elsevier Ltd. All rights reserved.
doi:10.1016/j.jeurceramsoc.2011.03.028

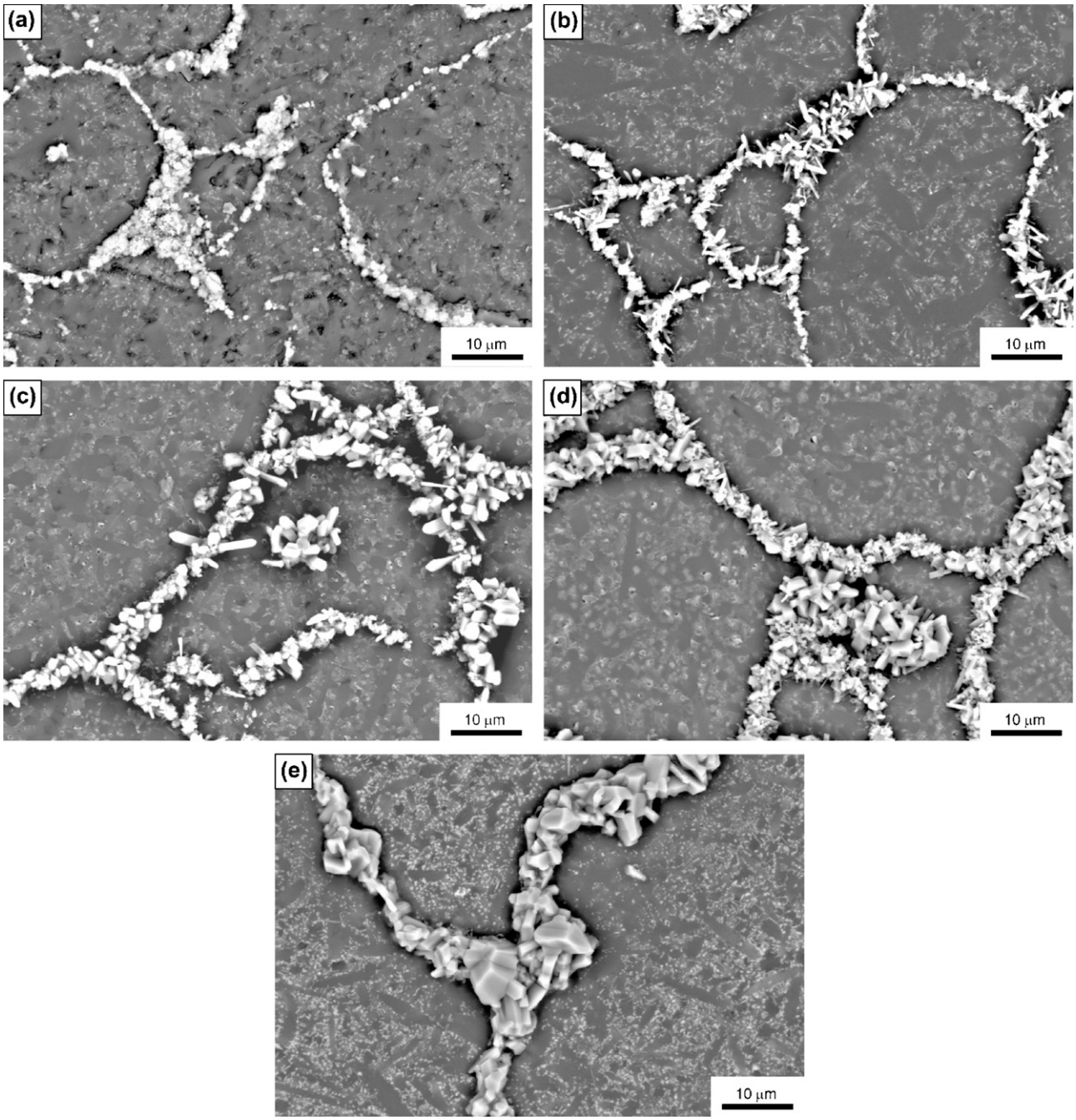

Fig. 1. Back-scattered SEM images of the composite containing 5 vol% TiCN oxidized at (a) 800 °C, (b) 900 °C, (c) 1000 °C, (d) 1100 °C and (e) 1200 °C for 2 h.

amounts of segregated network of TiCN particles was investigated by soaking the materials in air at different temperatures for short and long terms. The results are based on the thickness measurement of oxide scale from the surface and mass gain per unit area as a function of oxidation temperature.

2. Materials and methods

2.1. Production of composites

α/β SiAlON–TiCN composites were prepared by following a process[24] which is based on the dry mixing of different amounts of nano TiCN particles ranging from 2.5 to 10 vol% (60 nm APS, Merck) with spray dried SiAlON based granules of around 100 μm in diameter in a rotary plastic container. Coated granules were then uniaxial pressed in hardened steel die (50 mm × 50 mm × 4 mm) under ~220 MPa pressure. Sintering of the pellets was carried out in a BN crucible using a GPS furnace (FCT Anlagenbau GmbH, Germany), capable of operating at temperatures of up to 2000 °C in an inert atmosphere of up to 10 MPa pressure. A two-stage sintering schedule was employed, which included a first stage at a sintering temperature of 1940 °C for 60 min under a low nitrogen gas pressure of 0.2–0.5 MPa and a second stage at a sintering temperature

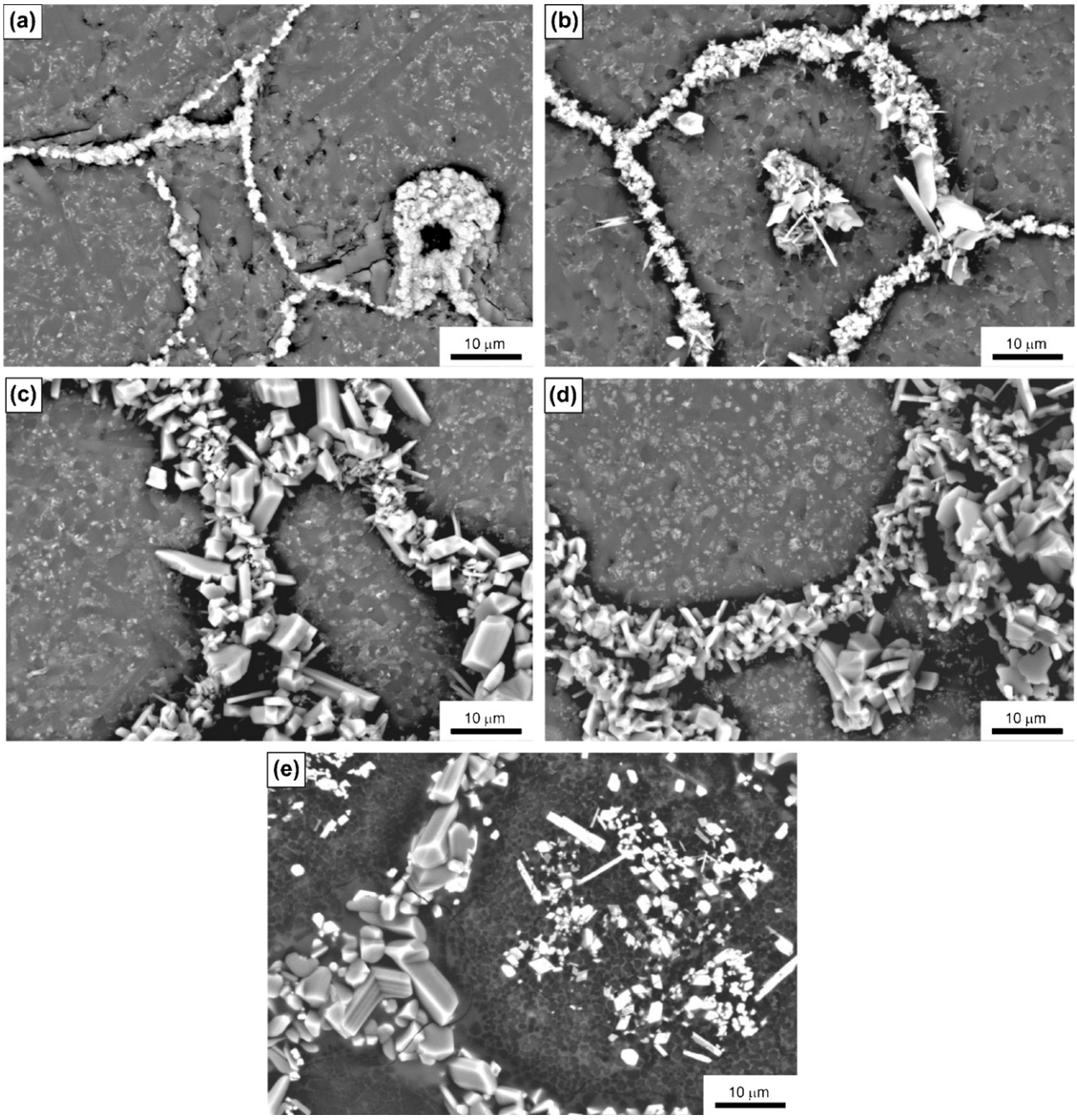

Fig. 2. Back-scattered SEM images of the composite containing 5 vol% TiCN oxidized at (a) 800 °C, (b) 900 °C, (c) 1000 °C, (d) 1100 °C and (e) 1200 °C for 48 h.

of 1990 °C for 60 min under a high nitrogen gas pressure of 10 MPa. The heating and cooling rates were kept at 10 °C/min.

2.2. Oxidation tests

After sintering, surface of the samples was ground using a diamond grinding wheel to remove sintering defects and to make the both surfaces parallel to each other. Samples were then cut in to rectangular bars (10 mm × 5 mm × 4 mm) and polished through a series of abrasives and polymer bounded disks followed by polishing with 6 μm and 1 μm diamond grinding pastes and finally ultrasonically cleaned in distilled water. Oxidation tests were carried out in a laboratory furnace in air at temperatures of 800, 900, 1000, 1100 and 1200 °C for 2 and 48 h.

2.3. Characterisation of the oxidized samples

The samples were carefully weighed before and after oxidation tests using four digit scale to follow the mass change resulted by the oxidation reactions. Phase identification of the samples was performed by X-ray diffractometer (Rigaku Rint 2200, Japan) with Ni-filtered Cu Kα radiation of wavelength 1.5418 Å.

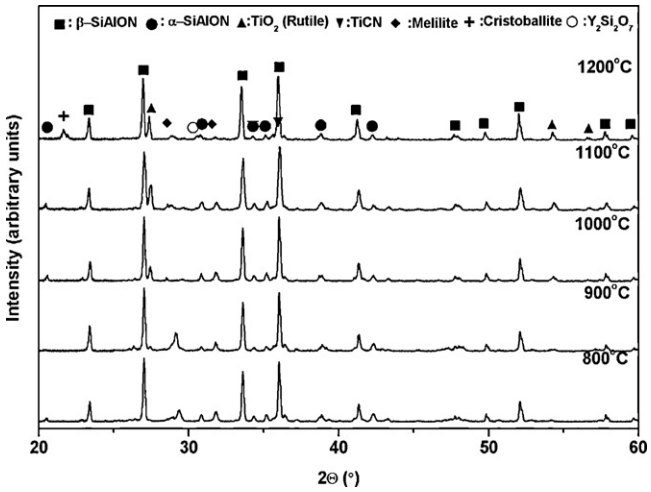

Fig. 3. Representative XRD spectra of the 10 vol% TiCN containing composite oxidized at 800–1200 °C for 2 h.

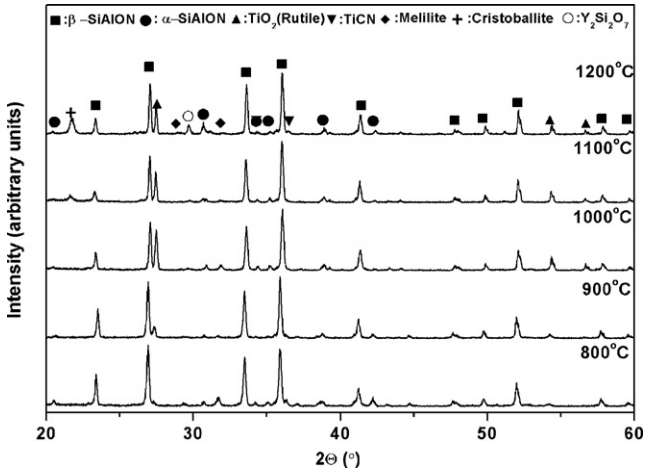

Fig. 4. Representative XRD spectra of the 10 vol% TiCN containing composite oxidized at 800–1200 °C for 48 h.

In order to identify the oxidation products and their penetration zone from the surface to inner parts, surfaces and the cross-sections of the oxidized samples were examined by scanning electron microscopy (FESEM, Supra 50 VP, Zeiss-Germany) equipped with an energy dispersive X-ray spectrometer (EDX, Oxford Instruments). The weight gain and loss $\Delta W/S$ (mg/cm^2) of the samples exposed to oxidation were recorded after every oxidation test.

3. Results and discussion

3.1. Surface analysis

Back-scattered scanning electron microscopy (BE-SEM) images of the 5 vol% TiCN containing samples oxidized at 800–1200 °C for 2 and 48 h given in Figs. 1 and 2, respectively. These micrographs reveal the surface morphology which is changed as a result of the oxidation reactions. Brighter regions in the images show the formation of TiO_2 crystals on the surfaces of the TiCN particles at 800 °C according to the reaction:

$$TiCN_{(s)} + 2O_{2(g)} \rightarrow TiO_{2(s)} + CO_{2(g)} + N_{2(g)} \quad (1)$$

However, there are still some unreacted particles which are seen as darker regions on the surfaces. It was determined that the types of the phases formed on the surface of the samples as a result of the oxidation are independent from the TiCN amounts. XRD analysis of the 10 vol% TiCN coated sample also supports both the TiO_2 formation and the presence of the retained TiCN particles (Figs. 3 and 4). When the soaking time was extended to 48 h, the population of the TiO_2 crystals increased; however, the crystal size maintained almost the same (Fig. 2a), which means that the grain growth of the TiO_2 crystals is mostly controlled by the temperature rather than time.

At 900 °C, it is obvious that TiO_2 crystals start to grow in their faceted low energy morphology as in agreement with the relevant study.[17] Especially in the long term oxidation, some crystals show exaggerated grain growth while SiAlON matrix surface still remains unchanged (Figs. 1b and 2b).

As the temperature is increased to 1000 °C, small TiO_2 crystals disappear and the larger TiO_2 crystals continue to grow. The oxidation begins to occur not only by the diffusion of oxygen through the inner TiCN particles, but also by the dissolution of TiO_2 in grain boundary viscous liquid. Oxidation of SiAlON is controlled by oxygen diffusion through SiO_2.[18] In addition to growth of the TiO_2 crystals, Figs. 1c and 2c show some glassy bubble-like SiO_2 and oxynitride formations around the SiAlON grains. This is due to the oxidation of intergranular phase in SiAlON composition according to the reactions[16]:

$$Si_3N_{4(s)} + 3O_{2(g)} \rightarrow 3SiO_{2(s)} + 2N_{2(g)} \quad (2)$$

$$SiN_xO_{y(s)} + (1/2)O_{2(g)} \rightarrow SiN_{x-1}O_{y+1(s)} + (1/2)N_{2(g)} \quad (3)$$

EDX analysis indicated that this glassy region consists of Y, Si, O and additional Ti which probably diffused through the grain boundary phase during sintering. This EDX result is also in agreement with the work done by Bracisiewicz et al.[16]

At 1100 °C, the growth of the TiO_2 crystals progresses further. Moreover, the oxidation of grain boundary phase around the SiAlON particles becomes more significant in the case of 48 h oxidation (Fig. 2d). Some small crystals in dendritic shape are also formed as a result of a possible reaction between SiO_2 induced by the oxidation of SiAlON and Y_2O_3 given in (4):

$$2SiO_{2(s)} + Y_2O_{3(s)} \rightarrow Y_2Si_2O_{7(s)} \quad (4)$$

Dissolution of TiO_2 into the grain boundary glassy phase causes to the formation of $Y_2Ti_2O_7$ in the same manner. The XRD spectrum in Fig. 3 show the peaks of SiO_2 (cristobalite) and $Y_2Si_2O_7/Y_2Ti_2O_7$ as in agreement with the SEM and EDX results.

At 1200 °C, needle-like $Y_2Si_2O_7/Y_2Ti_2O_7$ crystals become apparent on the surface of the SiAlON grains which are covered by equiaxed cristobalite grains (Fig. 1e and 2e). The intensities of (1 1 0) peak of rutile and (1 0 1) peak of cristobalite increase due to the increasing amount of these phases, as shown in Figs. 3 and 4. Moreover, some cracks are observed at the interface between the TiO_2 crystals and the surface oxides of the SiAlON particles due to the thermal expansion coefficient

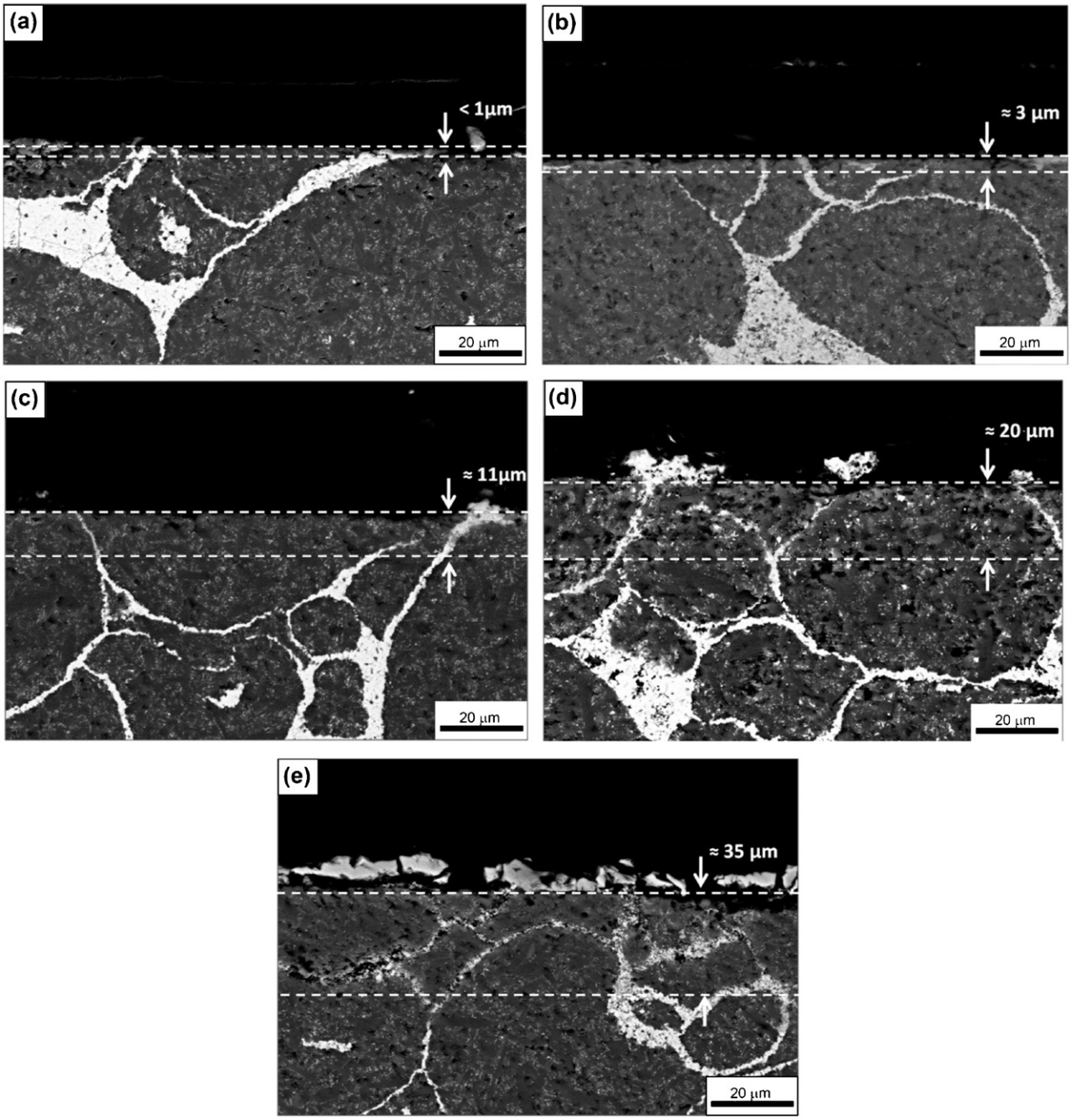

Fig. 5. Back-scattered SEM images of 10 vol% TiCN containing composite oxidized at (a) 800 °C, (b) 900 °C, (c) 1000 °C, (d) 1100 °C and (e) 1200 °C for 2 h.

mismatch of the phases and the volume expansion induced by the transformation of TiCN to TiO_2.

3.2. Cross-sectional analysis

The cross-sections of the composites were carefully characterised by SEM and mapping technique of EDX analysis to clarify the oxide scale thickness and the phase changes through the sample from the surface to the inside depending on the oxidation temperature. Figs. 5 and 6 show the cross-sectional BE-SEM micrographs of the 10 vol% of TiCN containing SiAlON composites oxidized for 2 and 48 h, respectively. The graph, shown in Fig. 7, summarizes the oxidized scale thicknesses of the composites for short and long term oxidation treatments.

After 2 h oxidation at 800 °C, no surface oxide scale could be observed. Since TiCN particles start to oxidize partially from the surfaces, it is difficult to recognize submicron scale thickness (Fig. 5a). Longer soaking time, however, causes an increase in the transformation of TiCN to TiO_2. Therefore, a light gray TiO_2 scale connected to the inner TiCN network (brighter region) was formed in an approximately 10 μm thickness.

At 900 °C, TiO_2 scale thickness is 3–5 μm for short term oxidation (Fig. 5b) whereas 15–20 μm for long term treatment

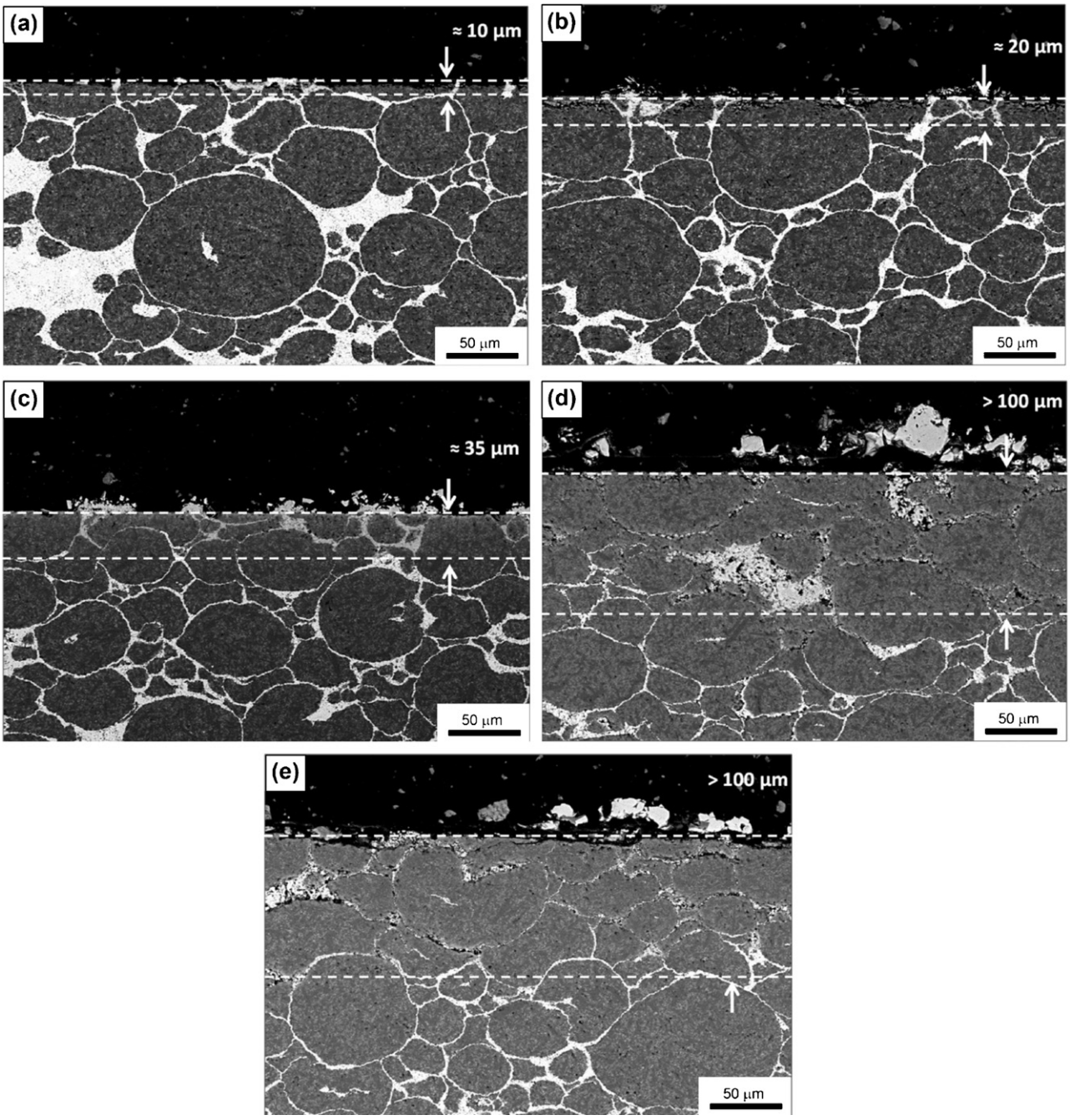

Fig. 6. Back-scattered SEM images of 10 vol% TiCN containing composite oxidized at (a) 800 °C, (b) 900 °C, (c) 1000 °C, (d) 1100 °C and (e) 1200 °C for 48 h.

(Fig. 6b). Oxidation still occurs by means of diffusion of oxygen atoms through the previously formed TiO_2.[15,16]

When the temperature is increased to 1000 °C, penetration zone still increases for both short and long terms. Due to the softening of the grain boundary phase, TiO_2 particles start to migrate through the channels open to the surface. At the temperature above the glass transition temperature, dissolution and transportation process of Ti in the intergranular glass plays an important role on the oxidation. Chemical potential gradient of oxygen (μO_2) on the grain boundary glass causes to formation of an oxygen flux along the grain boundaries. TiCN particles, which are connected to the SiAlON grain boundaries, are oxidized by the oxygen transported in liquid glass. Moreover, this chemical potential gradient of oxygen acts also as driving force for the diffusion of components of liquid towards to the surface, where the μO_2 is high. Among the components of grain boundary phase (Y, Sm, Ca, Al, Si and Ti), Ti is the fastest element so that the surface is covered by TiO_2. Migrated TiO_2 particles leave porosity on the oxidation zone.[17]

At 1100 °C, Ti migration towards the surface is severe. The oxidation of TiCN particles starts to be controlled by oxygen diffusion through TiO_2 and porosity towards inner TiCN particles.[18] Oxidation scale also increases considerably up to 20 μm for short term (Fig. 5d) and higher than 100 μm for long

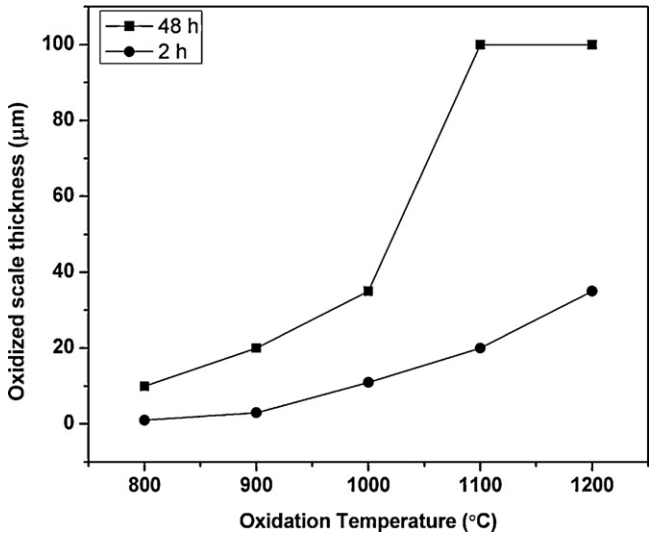

Fig. 7. Change in thickness of oxidation layer of 10 vol% TiCN containing composites for 2 and 48 h.

term oxidation (Fig. 6d). It is proposed that the structure of TiCN particles which are in contact, creates a path for oxygen diffusion to the inner particles. Therefore, TiO_2 migration from the deeper regions occurs (up to 100 μm) in the case of the segregated network composites in comparison to the particle dispersed counterparts (up to 50 μm).[15,18] Thus, there are large TiO_2 crystals easily clustered at the opening points of the network on the surface.

At 1200 °C, the activity of Ti decreases in comparison to the initial temperature (≈1000 °C) due to the depletion of TiCN and the formation of viscous liquid which reduces the oxygen flux by filling the pores in segregated channels and the surfaces. Oxidation is determined by the diffusion of oxygen into this continuous oxide layer, which is slower than that of in TiO_2. Therefore, the oxide scale thickness in Fig. 6e does not show a considerable change due to the growth of rather compact and protective surface oxide scale.

3.3. Mass change

2 h soaking time, for which the short term oxidation test was carried out, is not sufficient to cause any detectable mass gain in the samples. On the other hand, for the long term oxidation test (48 h), due to the significant oxidation reactions from (1)–(4), a considerable amount of oxides was formed. Fig. 8 shows the mass gain per unit area of the composites depending on the oxidation temperature.

It could be noted that between the temperatures of 800 and 1000 °C, all the composites show similar linear mass gain behavior because of the TiO_2 formation as a result of the diffusion of oxygen through the TiO_2 crystals and unreacted TiCN particles. Above 1000 °C, in addition to the reaction (1), contribution of reactions (2) and (3) takes place. Due to the mechanism change above 1000 °C, mass gain diagrams for 7.5 and 10 vol% TiCN coated composites show an exponential increase rather than a linear behavior.

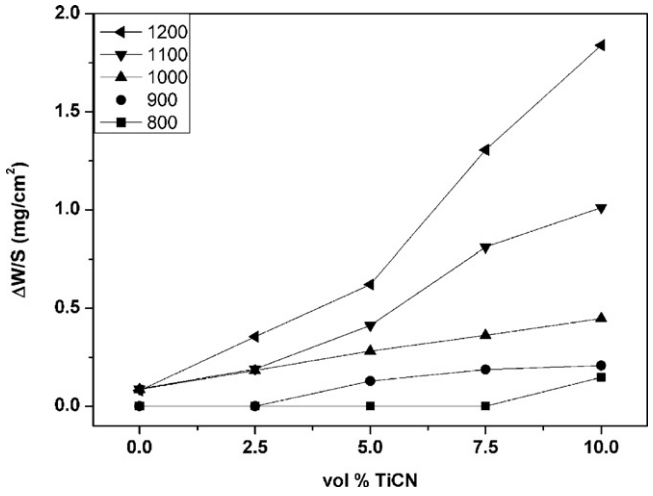

Fig. 8. Mass change per unit area of the composite materials oxidized for 48 h. depending on the oxidation temperature.

3.4. Oxidation kinetics

The oxidation of Si_3N_4/SiAlON[25–29] and TiCN/TiN[30,31] is diffusion controlled processes and therefore, the oxide scale thickness and the weight change can be expressed by the parabolic rate law:

$$(W \quad \text{or} \quad d)^2 = kt$$

where, t is the oxidation time and equals to 48 h, k is the oxidation rate constant. W and d are the mass gain per unit area and oxide scale thickness, respectively. Parabolic rate constants were calculated in two different ways;one is from the oxidized scale thicknesses and the other is from the weight changes of 10 vol% TiCN containing samples given in Figs. 7 and 8, respectively. By plotting the natural logarithm of oxidation rate constants ($\ln K$) vs T^{-1} (K), the temperature coefficients of oxidation rate (Ea) were obtained from the slope of Arrhenius plots which are given in Fig. 9.

It is expected that the activation energies calculated from weight change and scale thickness between 800 and 900 °C

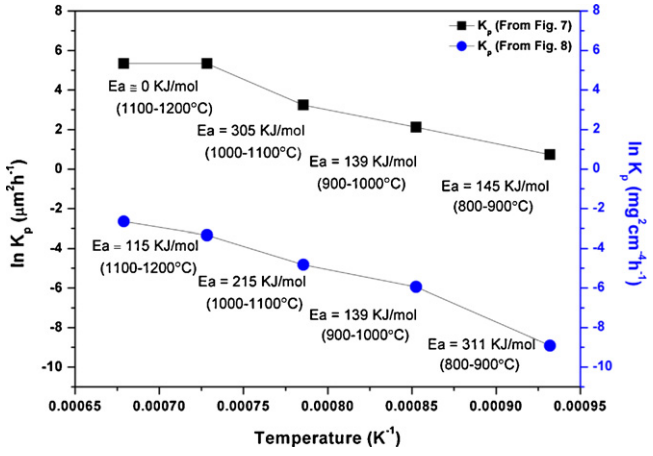

Fig. 9. Influence of temperature on the rate constants (K) obtained from weight change and oxidized scale thickness of 10 vol% TiCN containing sample.

should ideally be equal to each other since the only mechanism is the oxygen diffusion through TiCN particles. This is true in an ideal case at which the TiCN particles cover the SiAlON granules almost in a uniform thickness without forming large agglomerates. For 5 vol% TiCN containing composite which shows the most ideal segregation around the granules, the activation energies calculated from Figs. 7 and 8 are very close to each other between 800 and 1000 °C (between 800 and 900 °C, 145 kJ/mol from oxide thickness and 156 kJ/mol from weight change; between 900 and 1000 °C, 139 kJ/mol from oxide thickness and 107 kJ/mol from weight change). However, the *Ea* between 800 and 900 °C calculated from weight change is approximately double of *Ea* calculated from oxide scale thickness for 10 vol% TiCN due to large TiCN clusters (see Fig. 6) that cause higher formation of rutile phase in a certain oxygen penetration zone. Therefore, the differences between *Ea* values calculated from oxide scale thickness and weight change are directly related to the quantity of agglomeration in the zone that oxygen can penetrate. Between 900 and 1000 °C, the *Ea* values are equal.

Between 1000 and 1100 °C, the oxidation mechanism becomes complicated, since more than one oxidation processes take place. In addition to the oxygen diffusion through rutile, Ti starts to dissolve in softened glassy phase and migrate through the surface quickly. This mechanism causes to a sharp increase in oxidized scale thickness. The activation energies for this process were calculated as 305 kJ/mol. The sample weight is changed by both TiO_2 formation and oxide products resulted by Eqs. (2) and (3). The temperature coefficient of oxidation rate was found to be 215 kJ/mol for this temperature range.

At the final stage of the oxidation between 1100 and 1200 °C, the oxidized scale thickness is almost constant due to the protective viscous liquid formed by the oxidation of SiAlON matrix. The oxidation is mainly controlled by diffusion of oxygen through the glassy phase formed around the SiAlON particles and *Ea* value is 115 kJ/mol between this temperature ranges.

4. Conclusions

α/β SiAlON composites with a segregated network of TiCN particulates were oxidized at 800–1200 °C for 2 and 48 h in air. It was found that the oxidation for 2 h does not cause any detectable weight change due to the insufficient oxidation reactions. Since the amount of TiCN is lower (between 2.5 and 10 vol%) in comparison to the particulate reinforced composites (generally 20–40 vol%), it becomes also difficult to follow the weight changes in the investigated composites. In long term oxidation, up to 1000 °C, the samples gain weight due to the transformation of TiCN to TiO_2. After 1000 °C, in addition to the formation of TiO_2, oxide phases are formed as a result of the oxidation of the SiAlON matrix and these phases change the mass gain plot from linear to exponential.

Surface and cross-sectional investigation of the composites under SEM revealed that the oxidation is controlled by the diffusion of oxygen through rutile phase up to 1000 °C and the scale thickness increases gradually. After formation of a liquid phase, oxidation mechanism changes to Ti diffusion via dissolution into the glassy phase and precipitation on the surface. At the beginning of this stage, at 1000 and 1100 °C, Ti migration through the surface is very fast and causes a rapid increase in oxide scale thickness and in the amount of porosity. After 1100 °C, in addition to the formation of rutile crystals, cristobalite and $Y_2Si_2O_7/Y_2Ti_2O_7$ phases crystallize on the surface of the SiAlON matrix. Since these crystals behave as a protective layer against to oxygen penetration towards the inner part of the composite, the oxide scale thickness does not change much between 1100 and 1200 °C.

Oxidation rate constants obtained from mass change and oxidation thicknesses are almost equal to each other at temperatures lower than 1000 °C. However, agglomerates of TiCN particles around spray-dried granules during mechanical mixing process cause some deviations in *Ea* values. Between 1000 and 1100 °C, more than one oxidation mechanisms are active so that the calculated *Ea* values are equal to the sum of these different oxidation mechanisms. Above 1100 °C, oxidation process is mainly controlled by the oxygen diffusion through the glassy phase around the SiAlON particles and the *Ea* value of this process is 115 kJ/mol.

References

1. Gogotsi YG. Particulate silicon nitride based composites. *J Mater Sci* 1994;**29**:2541–56.
2. Sajgalik P, Hnatko M, Lofaj F, Hvizdos P, Dusza J, Warbichler P, et al. SiC/Si_3N_4 nano/micro-composite: processing, RT and HT mechanical properties. *J Eur Ceram Soc* 2000;**20**:453–62.
3. Shiogai T, Tsukamoto K, Sashida N. Creep properties of (Si–Al–O–N)–SiC whisker composites. *J Mater Sci* 1998;**33**:769–73.
4. Bitterlich B, Bitsch S, Friederich K. SiAlON based ceramic cutting tools. *J Eur Ceram Soc* 2008;**28**:989–94.
5. Huang JL, Kuo FJ, Chen SY. Investigation of microstructure and crack behaviours in hot-pressed TiB_2–Si_3N_4 composites. *Mater Sci Eng A* 1994;**174**:157–64.
6. Wani MF, Khan ZA, Hadfield M. Effect of sintering additives and reinforcement on microhardness values of Si_3N_4 ceramics and composites. *J Adv Res Mech Eng* 2010;**1**:52–9.
7. Jiang D, Vanmeensel K, Vleugels J, Van der Biest O. Si_3N_4-based composites with micron and nano-sized $TiC_{0.5}N_{0.5}$ particles. *Sil Ind* 2004;**69**(Special Issue):7–8.
8. Bellosi A, Guicciardi S, Tampieri A. Development and characterization of electroconductive Si_3N_4–TiN composites. *J Eur Ceram Soc* 1992;**9**(2):83–93.
9. Guo Z, Blugan G, Kirchner R, Reece M, Graule T, Kuebler J. Microstructure and electrical properties of Si_3N_4–TiN composites sintered by hot pressing and spark plasma sintering. *Ceram Int* 2007;**33**:1223–9.
10. Sawaguchi A, Toda K, Niihara K. Mechanical and electrical properties of silicon nitride-silicon carbide nanocomposite material. *J Am Ceram Soc* 1991;**74**(5):1142–4.
11. Kim WJ, Taya M, Yamada K, Kamiya N. Percolation study on electrical resistivity of SiC/Si_3N_4 composites with segregated distribution. *J Appl Phys* 1998;**83**(5):2593–8.
12. Yamada K, Kamiya N. High temperature mechanical properties of Si_3N_4–$MoSi_2$ and Si_3N_4–SiC composites with network structures of second phase. *Mater Sci Eng A* 1999;**261**:270–7.
13. Petrovsky VY, Rak RZ. Densification, microstructure and properties of electroconductive Si_3N_4–TaN composites. Part II: electrical and mechanical properties. *J Eur Ceram Soc* 2001;**21**:237–44.
14. Medri V, Bracisiewicz M, Krnel K, Winterhalter F, Bellosi A. Degradation of mechanical and electrical properties after long-term oxidation and corrosion of non-oxide structural ceramic composites. *J Eur Ceram Soc* 2005;**25**:1723–31.

15. Bellosi A, Tampieri A, Liu YZ. Oxidation behavior of electroconductive Si_3N_4–TiN composites. *Mater Sci Eng A* 1990;**127**:115–22.
16. Bracisiewicz M, Medri V, Bellosi A. Factors inducing degradation of properties after long term oxidation of Si_3N_4–TiN electroconductive composites. *Appl Surf Sci* 2002;**202**:139–49.
17. Feldhoff A, Trichet MF, Mazerolles L, Backhaus-Ricoult M. Electron microscopy study on the high-temperature oxidation of Si_3N_4–TiN ceramics: in situ and ex situ investigations. *J Eur Ceram Soc* 2005;**25**:1733–42.
18. Deschaux-Beaume F, Frety N, Cutard T, Colin C. Oxidation modeling of a Si_3N_4–TiN composite: comparison between experiment and kinetic models. *Ceram Int* 2009;**35**:1709–18.
19. Klemm H, Schubert C. Silicon nitride/molybdenum disilicide composite with superior long-term oxidation resistance at 1500 °C. *J Am Ceram Soc* 2001;**84**:2430–2.
20. Klemm H, Tangermann K, Schubert C, Hermel W. Influence of molybdenum silicide additions on high-temperature oxidation resistance of silicon nitride materials. *J Am Ceram Soc* 1996;**79**:2429–35.
21. Kawano S, Takahashi J, Shimada S. The preparation and spark plasma sintering of silicon nitride-based materials coated with nano-sized TiN. *J Eur Ceram Soc* 2004;**24**:309–12.
22. Krnel K, Maglica A, Kosmac T. β-SiAlON/TiN nanocomposites prepared from TiO_2-coated Si_3N_4 powder. *J Eur Ceram Soc* 2008;**28**:953–7.
23. Gao L, Li L, Kusunose T, Niihara K. Preparation and properties of TiN–Si_3N_4 composite. *J Eur Ceram Soc* 2004;**24**(2):381–6.
24. Ayas E, Kara A. Novel electrically conductive α–β SiAlON/TiCN composites. *J Eur Ceram Soc* 2011;**31**:903–11.
25. Houjou K, Ando K, Chu MC, Liu SP, Sato S. Effect of sintering additives on the oxidation behaviour of Si_3N_4 ceramics at 1300 °C. *J Eur Ceram Soc* 2005;**25**:559–67.
26. Tong X, Li J, Yang X, Lin H, Guo G, He M. Mechanical property and oxidation behaviour of self-reinforced Si_3N_4 doped with Re_2O_3 (Re = Yb, Lu). *J Am Ceram Soc* 2006;**89**(5):1730–2.
27. Hou XM, Chou KC, Li FS. Some new perspectives on oxidation kinetics of SiAlON materials. *J Eur Ceram Soc* 2008;**28**:1243–9.
28. Nordberg L, Nygren M. Stability and oxidation properties of RE-α-SiAlON ceramics (RE = Y, Nd, Sm, Yb). *J Am Ceram Soc* 1998;**81**(6):1461–70.
29. MacKenzie K, Sheppard CM, Barris GC, Mills AM, Shimada S, Kiyono H. Kinetics and mechanism of thermal oxidation of SiAlON ceramic powders. *Thermochim Acta* 1998;**318**:91–100.
30. Diserens M, Patscheider J, Levy F. Mechanical properties and oxidation resistance of nanocomposite TiN–SiN_x physical-vapor-deposited thin films. *Surf Coating Technol* 1999;**120–121**:158–65.
31. Llauro G, Gourbilleau F, Sibieude F, Hillel R. Oxidation behaviour of CVD TiN–Ti_5Si_3 composite coatings. *Thin Solid Films* 1998;**315**:336–44.